APOGEE spectroscopic evidence for chemical anomalies in dwarf galaxies: The case of M 54 and Sagittarius

José Fernández-Trincado, Timothy Beers, Dante Minniti, Christian Moni Bidin, Beatriz Barbuy, Sandro Villanova, Doug Geisler, Richard Lane, Alexandre Roman-Lopes, Dmitry Bizyaev

A&A 648, A70 (2021)
https://doi.org/10.1051/0004-6361/202140306

Astronomy & Astrophysics

APOGEE spectroscopic evidence for chemical anomalies in dwarf galaxies: The case of M 54 and Sagittarius

José G. Fernández-Trincado[1,2,3], Timothy C. Beers[4], Dante Minniti[5,6], Christian Moni Bidin[7], Beatriz Barbuy[8], Sandro Villanova[9], Doug Geisler[9,10,11], Richard R. Lane[1], Alexandre Roman-Lopes[10], and Dmitry Bizyaev[12,13]

[1] Instituto de Astronomía y Ciencias Planetarias, Universidad de Atacama, Copayapu 485, Copiapó, Chile
e-mail: jose.fernandez@uda.cl, jfernandezt87@gmail.com
[2] Institut Utinam, CNRS UMR 6213, Université Bourgogne-Franche-Comté, OSU THETA Franche-Comté, Observatoire de Besançon, BP 1615, 25010 Besançon Cedex, France
[3] Centro de Investigación en Astronomía, Universidad Bernardo O Higgins, Avenida Viel 1497, Santiago, Chile
[4] Department of Physics and JINA Center for the Evolution of the Elements, University of Notre Dame, Notre Dame, IN 46556, USA
[5] Depto. de Cs. Físicas, Facultad de Ciencias Exactas, Universidad Andrés Bello, Av. Fernández Concha 700, Las Condes, Santiago, Chile
[6] Vatican Observatory, 00120 Vatican City State, Italy
[7] Instituto de Astronomía, Universidad Católica del Norte, Av. Angamos 0610, Antofagasta, Chile
[8] Universidade de São Paulo, IAG, Rua do Matão 1226, Cidade Universitária, São Paulo 05508-900, Brazil
[9] Departamento de Astronomía, Casilla 160-C, Universidad de Concepción, Concepción, Chile
[10] Departamento de Astronomía, Universidad de La Serena, 1700000 La Serena, Chile
[11] Instituto de Investigación Multidisciplinario en Ciencia y Tecnología, Universidad de La Serena, Benavente 980, La Serena, Chile
[12] Apache Point Observatory and New Mexico State University, Sunspot, NM 88349, USA
[13] Sternberg Astronomical Institute, Moscow State University, Moscow, Russia

Received 9 January 2021 / Accepted 8 February 2021

ABSTRACT

We present evidence for globular cluster stellar debris in a dwarf galaxy system (Sagittarius; Sgr) based on an analysis of high-resolution *H*-band spectra from the Apache Point Observatory Galactic Evolution Experiment (APOGEE) survey. We add [N/Fe], [Ti/Fe], and [Ni/Fe] abundance ratios to the existing sample of potential members of M 54; this is the first time that [N/Fe] abundances are derived for a large number of stars in M 54. Our study reveals the existence of a significant population of nitrogen- (with a large spread, $\gtrsim$1 dex) and aluminum-enriched stars with moderate Mg depletions in the core of the M 54+Sgr system, which share the light element anomalies characteristic of second-generation globular cluster stars (GC), thus tracing the typical phenomenon of multiple stellar populations seen in other Galactic GCs at similar metallicity, confirming earlier results based on the Na-O anti-correlation. We further show that most of the stars in M 54 exhibit different chemical patterns evidently not present in Sgr field stars. Furthermore, we report the serendipitous discovery of a nitrogen-enhanced extra-tidal star that has GC second-generation-like chemical patterns for which both chemical and kinematic evidence are commensurate with the hypothesis that the star has been ejected from M 54. Our findings support the existence of chemical anomalies associated with likely tidally shredded GCs that are in dwarf galaxies in the Local Group. These findings motivate future searches for such bona fide stars along other known Milky Way streams.

Key words. stars: abundances – stars: chemically peculiar – globular clusters: individual: M 54 – techniques: spectroscopic

1. Introduction

The Sagittarius (Sgr) dwarf spheroidal (dSph) galaxy is one of the closest massive satellites of the Milky Way (MW; Ibata et al. 1994), has yielded a wealth of observational evidence of ongoing accretion by the MW in the form of persistent stellar debris and tidal streams discovered by Mateo et al. (1996), and has been extensively studied with photometric and spectroscopic observations over a huge range of distances (∼10–100 kpc; see, e.g., Ibata et al. 2001; de Boer et al. 2015). These studies have used different stellar tracers, including carbon stars (Totten & Irwin 1998), the first all-sky map of the tails using 2MASS M-giants (Majewski et al. 2003), red clump stars (Correnti et al. 2010), RR Lyrae stars (Newberg et al. 2003; Ramos et al. 2020), and CN-strong stars (Hanke et al. 2020), among other tracers, usually in small patches along the stream (see, e.g., Li et al. 2019). These studies have been followed up by numerical studies (see, e.g., Law et al. 2005; Vasiliev et al. 2021) and by the use of precise astrometry from the *Gaia* second data release (*Gaia* DR2; Gaia Collaboration 2018a) based on proper motions alone (Antoja et al. 2020). Its proximity provides a unique laboratory to study accretion in detail, through the tidally stripped streams that outflow from the Sgr system (Hasselquist et al. 2017, 2019; Hayes et al. 2020).

As a natural result of such an accretion event, there is a claim in the literature that not only field stars but also GCs have been accreted (see, e.g., Massari et al. 2019). Some have been speculated to be lost in the disruption process and may lie immersed in the Sgr stream. Candidates include M 54, Terzan 7, Arp 2, Terzan 8, Pal 12, Whiting 1, NGC 2419, NGC 6534,

and NGC 4147 (e.g., Law & Majewski 2010; Bellazzini et al. 2020), but a firm connection is still under debate (e.g., Villanova et al. 2016; Tang et al. 2018; Huang & Koposov 2021; Yuan et al. 2020). In this context, "chemical tagging" (e.g., Freeman & Bland-Hawthorn 2002), which is based on the principle that the photospheric chemical compositions of stars reflect the site of their formation, is a promising route to investigate this question.

While the abundances of light and heavy elements for individual stars in GCs have been widely explored (e.g., Pancino et al. 2017; Mészáros et al. 2020), little is known about these abundances in disrupted GCs likely associated with the closest dwarf galaxies, such as Sgr (Karlsson et al. 2012). Although some evidence for chemical anomalies has been detected toward the inner bulge and halo of the MW (see, e.g., Fernández-Trincado et al. 2016, 2017; Recio-Blanco et al. 2017; Schiavon et al. 2017) and Local Group dwarf galaxies (see, e.g., Fernández-Trincado et al. 2020a), suggesting the presence of GCs in the form of disrupted remnants, alternative ways to produce these stars have recently been discussed (Bekki 2019).

This paper is outlined as follows. The high-resolution spectroscopic observations are discussed in Sect. 2. Section 2.1 describes the sample associated with M 54, including a comparison with data from the literature. Section 3 presents our estimated stellar parameters and derived chemical-abundance determinations. Section 4 discusses the results, and our concluding remarks are presented in Sect. 5.

2. Data

We make use of the internal data set, which includes all data taken through March 2020, of the second-generation Apache Point Observatory Galactic Evolution Experiment (APOGEE-2; Majewski et al. 2017). The data set includes the first observations from the *Irénée du Pont* 2.5 m Telescope at Las Campanas Observatory (APO-2S; Bowen & Vaughan 1973) in the Southern Hemisphere (Chile) and more observations from the Sloan 2.5 m Telescope at Apache Point Observatory (APO-2N; Gunn et al. 2006) in the Northern Hemisphere (New Mexico). The survey operates with two nearly identical spectrographs (Eisenstein et al. 2011; Wilson et al. 2012, 2019), collecting high-resolution ($R \sim 22\,000$) spectra in the near-infrared H band (1.5145–1.6960 μm, vacuum wavelengths). This data set provides stellar parameters, chemical abundances, and radial velocity (RV) information for more than 600 000 sources, which include ~437 000 targets from the 16th data release (DR16; Ahumada et al. 2020) of the fourth generation of the Sloan Digital Sky Survey (SDSS-IV; Blanton et al. 2017). The APOGEE-2 target selection is described in full detail in Zasowski et al. (2017; APOGEE-2), Santana et al. (in prep.; APO-2S), and Beaton et al. (in prep.; APO-2N).

The APOGEE-2 spectra were reduced (Nidever et al. 2015) and analyzed using the APOGEE Stellar Parameters and Chemical Abundance Pipeline (ASPCAP; García Pérez et al. 2016; Holtzman et al. 2015, 2018; Jönsson et al. 2018, 2020). The model grids for APOGEE-2 internal data set are based on a complete set of `MARCS` stellar atmospheres (Gustafsson et al. 2008), which now extend to effective temperatures as low as 3200 K, and spectral synthesis using the `Turbospectrum` code (Plez 2012). The APOGEE-2 spectra provide access to more than 26 chemical species, which are described in Smith et al. (2013), Shetrone et al. (2015), Hasselquist et al. (2016), Cunha et al. (2017), and Holtzman et al. (2018).

2.1. M 54 field

The APOGEE-2 field toward M 54 was previously examined in Mészáros et al. (2020) based on public DR16 spectra. In that work, 22 stars were identified as potential members linked to M 54 based in the APOGEE-2 radial velocities (Nidever et al. 2015). Stars with RV within $3\sigma_{\rm RV,cluster}$, metallicity within ±0.5 dex around the cluster average, proper motion from the *Gaia* Early Data Release 3 (*Gaia* EDR3; Gaia Collaboration 2021) within 2.5σ around the cluster average proper motion, and located inside the cluster tidal radius, $r_{\rm t} \lesssim 10$ arcmin (Harris 1996, 2010 edition) were classified as potential members of M 54. However, only 7 out of 22 stars were spectroscopically examined with the `BACCHUS` code in Masseron et al. (2016), since only these stars achieved a signal-to-noise ($S/N > 70$) sufficient to provide reliable abundance determinations.

The post-APOGEE DR16 data set provides incremental visits toward M 54, which has allowed us to increase the S/N for 20 out of 22 of the potential cluster members. As a result, nitrogen, titanium, and nickel abundances can be now obtained from the stronger absorption features (as shown for $^{12}C^{14}N$ lines in Fig. A.1) and other chemical species can also be studied.

Nataf et al. (2019), using APOGEE-2 DR14 data (Abolfathi et al. 2018) and abundance determinations from the `Payne` pipeline (Ting et al. 2019), have catalogued eight possible members from M 54. Two of those objects (2M18544275−3029012 and 2M18550740−3026052) were included in our study. The remaining six stars were rejected from our analysis for the following reasons. Six objects in Nataf et al. (2019) were found to have low S/N (<70) spectra, resulting in very uncertain CNO abundance ratios for many chemical species, since the molecular lines (^{16}OH, $^{12}C^{16}O$, and $^{12}C^{14}N$) are very weak. Secondly, six out of the eight objects in Nataf et al. (2019) exhibit [Fe/H] > −1.1 and were recently classified as Sgr stars (see, e.g., Hayes et al. 2020), which make them unlikely members of M 54.

In this study, we make use of the more recent spectra to examine the chemical composition of added stars to the abundance average of M 54. As in Mészáros et al. (2020), we also limit our discussion only to stars with $S/N > 70$.

2.2. Extra-tidal stars

We also report on the serendipitous discovery of two nitrogen-enhanced (N-rich) metal-poor stars beyond the tidal radius of M 54, as shown in panel a of Fig. 1. The APOGEE-2 stars in the stream+core Sgr system (see, e.g., Hasselquist et al. 2017, 2019; Hayes et al. 2020) are highlighted as black open star symbols in panel a of Fig. 1, while potential star members of the stream+core Sgr system from Antoja et al. (2020) are also shown in panel a of Fig. 1. It is important to note that the [Fe/H] abundance of APOGEE-2 Sgr stars are provided by the `ASPCAP` pipeline (see Hasselquist et al. 2017, 2019; Hayes et al. 2020). In order to compare with our [Fe/H] determinations, an offset of ~0.11 dex was applied to `ASPCAP` metallicities in panel d of Fig. 1, as suggested in Fernández-Trincado et al. (2020b).

Panels a–d of Fig. 1 reveal that one (2M18565969−3106454) of the newly discovered N-rich stars meets the minimum criterion to be considered a potential extra-tidal star that has likely escaped the cluster potential, while the second N-rich star (2M18533777−3129187) has physical properties that are clearly offset from the M 54 population. In particular, this star is brighter than the typical population of M 54 (see panel c in Fig. 1) and both proper motions and RV differ from the nominal proper

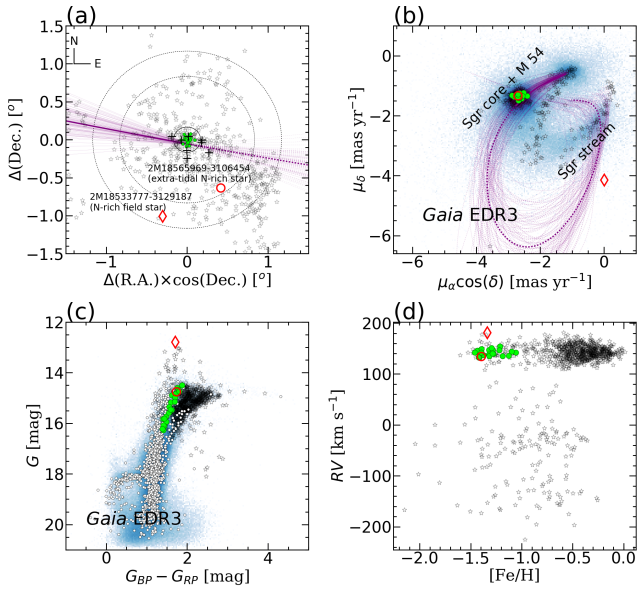

Fig. 1. Properties of the potential extra-tidal stars compared with likely members of M 54. *Panel a*: spatial positions of the stars in our sample, with the tidal radius (r_t = 10′) of M 54 over-plotted with a solid line. The open red symbols designate N-rich stars, the diamond symbol refers to a field star, and the open circle highlights the extra-tidal member of M 54. The lime circles designate the M 54 population analyzed in this work, while the black plus symbols designate the stars analyzed by Nataf et al. (2019). The empty gray star symbols designate the potential Sgr population from Hayes et al. (2020). The two concentric circles indicate 5 r_t and 7 r_t for reference. *Panel b*: *Gaia* EDR3 proper motions of stars that are associated with the Sgr stream: blue symbols for the Antoja et al. (2020) stars and open black star symbols for Hayes et al. (2020) stars. The orbital path of Sgr is shown by the dotted (backward) and solid (forward) purple line in *panels a and b*; the thick and thin lines show the central orbit, and an ensemble of 100 orbits that shows the more probable regions of the space, which are crossed more frequently by the simulated orbit, respectively. *Panel c*: color magnitude diagram from *Gaia* EDR3 photometry of our sample. The symbols are the same as in panels a and b, except the white circles, which denotes the M 54 members from *Gaia* EDR3, selected on proper motions and within 3′ from the cluster center. *Panel d*: radial velocities vs. [Fe/H] ratios determined from APOGEE-2/ASPCAP (black symbols) and our [Fe/H] ratio determinations from BACCHUS (green and red symbols) in the field around M 54. The [Fe/H] APOGEE-2/ASPCAP determinations are systematically offset by ∼0.11 dex to compare with our [Fe/H] BACCHUS determinations, as suggested in Fernández-Trincado et al. (2020b).

motion and RV of the cluster as shown in panels b and d of Fig. 1. It is likely that 2M18533777−3129187 is a foreground field star (hereafter N-rich field star).

3. Stellar parameters and chemical-abundance determinations

The chemical analysis is very similar to that carried out by Fernández-Trincado et al. (2019a,b,c,d, 2020c,a,b,d, 2021a). The stellar parameters ($T_{\rm eff}$, log g, and first guess on metallicity) for the 20 cluster members with $S/N > 70$ were extracted from Mészáros et al. (2020), while we adopted the atmospheric parameters from the uncalibrated post-APOGEE DR16 values for the two stars beyond the cluster tidal radius. The elemental abundances and final errors in [Fe/H] and [X/Fe], astrometric and kinematic properties of our sample are listed in Tables A.1–A.3, respectively.

A consistent chemical-abundance analysis was then carried out with the BACCHUS code (Masseron et al. 2016), from which we obtained the metallicities from Fe I lines, and abundances for 12 other chemical species belonging to the light- (C, N), α- (O, Mg, Si, Ca, and Ti), Fe-peak (Ni), odd-Z (Al, K) and s-process (Ce, Nd) elements.

4. Results and discussion

Panel a of Fig. 2 summarizes the chemical enrichment seen in M 54 stars analyzed in this work and draws a comparison with the Mészáros et al. (2020) determinations. The chemical composition of the two newly identified N-rich stars beyond the cluster tidal radius is also shown in the same figure. Overall, the chemical abundance of M 54 based on the added cluster stars is within the typical errors and does not affect the science results presented in Mészáros et al. (2020), while the two external N-rich stars share chemical patterns similar to the M 54 population.

For M 54, we find a mean metallicity ⟨[Fe/H]⟩ = −1.30 ± 0.12, which agrees well with Mészáros et al. (2020). The spread in [Fe/H] increased from 0.04 to 0.12 dex, but it is still smaller than that reported in Carretta et al. (2010). Even if the measured scatter is larger than that reported by Mészáros et al. (2020), this does not seem to indicate the presence of a significant spread in [Fe/H], and is similar to that observed in GCs at similar metallicity, such as M 10 (see, e.g., Mészáros et al. 2020). Nickel (an element that belongs to the Fe-group) exhibits a flat distribution as a function of [Fe/H], similar to that observed in Carretta et al. (2010) and at odds with that observed in Sgr stars. We note that in this work, and for the abundances described below, the number following the average abundance represents the one-sigma dispersion, not the error in the mean.

Regarding the other chemical species, we find excellent agreement with the values provided by Mészáros et al. (2020), as can be seen in panel a of Fig. 2, with the main difference that the added stars introduce a larger star-to-star scatter than previously measured. M 54 exhibits a modest enhancement in α-elements with mean values for [O/Fe], [Mg/Fe], [Si/Fe], [Ca/Fe], and [Ti/Fe]. These values are similar to that seen in halo GCs: ⟨[O/Fe]⟩ = +0.64 ± 0.36 (14 stars); ⟨[Mg/Fe]⟩ = +0.18 ± 0.11 (18 stars); ⟨[Si/Fe]⟩ = +0.26 ± 0.10 (20 stars); ⟨[Ca/Fe]⟩ = +0.25 ± 0.07 (16 stars); and the new measured ⟨[Ti/Fe]⟩ = +0.21 ± 0.21 (16 stars), indicating a fast enrichment provided by supernovae (SNe) II events. Mean values are in good agreement with Mészáros et al. (2020), with the exception of oxygen, which displays the larger star-to-star spread expected in likely second-generation stars.

We also find that the [O/Fe], [Mg/Fe], and [Si/Fe] ratios are almost flat as a function of the metallicity, while [Ca/Fe] and [Ti/Fe] ratios slightly increases as [Fe/H] increases, similar to the behaviour found by Carretta et al. (2010). On the contrary, the α-element trend observed in Sgr stars (see, e.g., Carretta et al. 2010; McWilliam et al. 2013; Hasselquist et al. 2017, 2019) differ from those seen in the population of M 54. Overall, the α-elements in the cluster are higher than seen in Sgr stars. In conclusion, the measured α-enrichment in this work supports the previous hypothesis suggesting that the α-element in M 54 stars formed before the typical e-folding time for SN Ia, thereby contributing their ejecta to the gas pool (e.g., Carretta et al. 2010).

We also found that some stars in M 54 appear to be quite Mg poor, with strong enrichment in aluminum and nitrogen, providing further evidence for the presence of second-generation stars in M 54, and the signature of very high temperatures achieved during H-burning (e.g., Carretta et al. 2010;

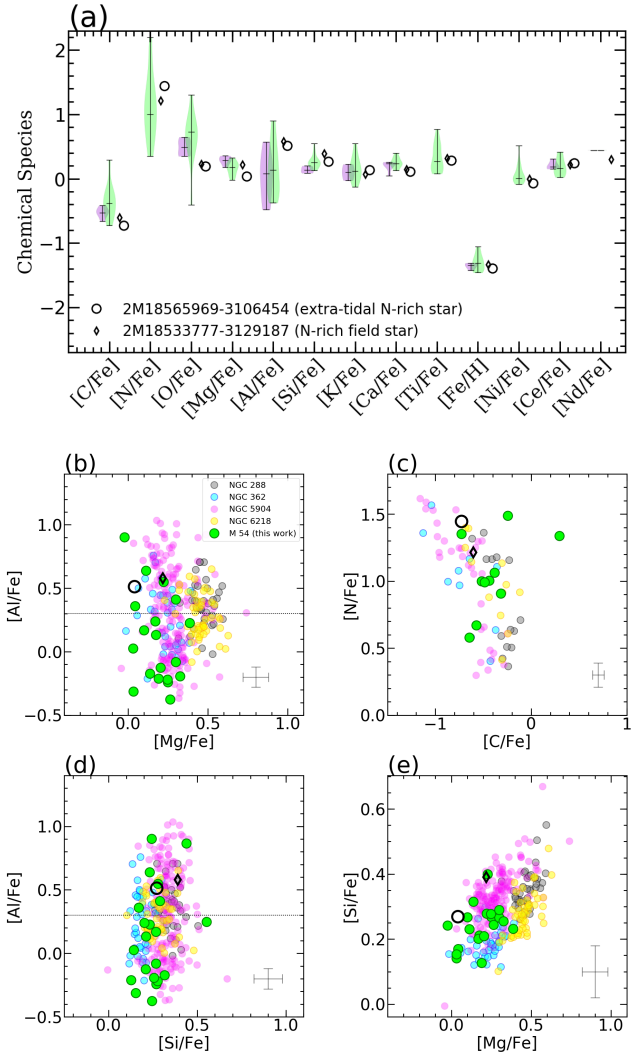

Fig. 2. BACCHUS elemental abundances. *Panel a*: observed [X/H] and [Fe/H] abundance-density estimation (violin representation) of M 54 stars and the observed abundance ratios of newly identified N-rich stars. The extra-tidal star from M 54 and a field star are highlighted with a black open circle and diamond, respectively. Each violin indicates the median and limits of the distribution with horizontal lines. The lime and dark violet violin representation refer to the abundance ratios of 20 stars (this work) and 7 stars from Mészáros et al. (2020), respectively. *Panels b–e*: distributions of light- (C,N), α- (Mg, Si) and odd-Z (Al) elements in different abundance planes. In each panel, the planes [Al/Fe] – [Mg/Fe], [N/Fe]–[C/Fe], [Al/Fe]–[Si/Fe], [Si/Fe]–[Mg/Fe] are shown, respectively, for GCs from Mészáros et al. (2020). The black dotted line at [Al/Fe] = +0.3 indicates the separation of FG and SG stars as proposed in Mészáros et al. (2020). The distribution of M 54 stars (lime squares) analyzed in this work are overlaid. The black open circle and diamond refer to the extra-tidal and field N-rich star, respectively. The plotted error bars show the typical abundance uncertainties.

Mészáros et al. 2020). The odd-Z elements (Al and K) in M 54 exhibit an average $\langle$[Al/Fe]$\rangle$ = +0.14 ± 0.37 (19 stars) and $\langle$[K/Fe]$\rangle$ = +0.15 ± 0.18 (17 stars); there is a clear anti-correlation in Al-Mg, as can be seen in in panel b of Fig. 2, where the moderate Mg depletions are related to the enrichment in Al abundances, as the result of the conversion of Mg into Al during the Mg-Al cycle (e.g., Carretta et al. 2010; Denissenkov et al. 2015; Renzini et al. 2015; Pancino et al. 2017). This pattern is evidently not present in the Sgr stars, where, on the contrary, ASPCAP Mg and Al abundances are positively correlated with each other (see, e.g., Hasselquist et al. 2017, 2019; Hayes et al. 2020).

We derived average abundances for C and N in M 54, of $\langle$[C/Fe]$\rangle$ = −0.36 ± 0.25 (13 stars) and $\langle$[N/Fe]$\rangle$ = +1.12 ± 0.48 (17 stars). Most of the stars in M 54 are C deficient ([C/Fe]$\lesssim$+0.3) and N enhanced ([N/Fe] > +0.5), but they do not exhibit the typical N-C anti-correlation (see panel c of Fig. 2) seen in other GCs at similar metallicity (e.g., Mészáros et al. 2020), most probably due the lack of stars with low nitrogen abundances. On the contrary, an apparent continuous distribution of N abundances is present in M 54. This result indicates the prevalence of the multiple-population phenomenon in M 54 as previously suggested in the literature (Carretta et al. 2010; Milone et al. 2017; Sills et al. 2019; Mészáros et al. 2020).

Additionally, we do not find any evidence for the presence of the K-Mg anti-correlation in M 54, as has been suggested to be present in a few Galactic GCs at similar metallicity (Mészáros et al. 2020). Furthermore, a Si-Al correlation is slightly evident in M 54, as shown in panel d of Fig. 2, and has a stubby Mg-Si distribution (see panel e of Fig. 2). This distribution is an indication of ^{28}Si production from the result of a secondary leakage in the main Mg-Al cycle, which is instead absent in the Sgr stars.

For the elements produced by neutron(n)-capture processes (Ce II and Nd II), we find on average $\langle$[Ce/Fe]$\rangle$ = +0.18 ± 0.13 (10 stars) and [Nd/Fe] = +0.44 (1 star). Overall, M 54 exhibits a modest enrichment in s-process elements, with a few stars as enhanced as +0.4, similar to that observed in Galactic GCs at similar metallicity (see, e.g., Mészáros et al. 2020), suggesting that it is possible that the s-process enrichment was produced by a source other than the progenitor of the Mg-Al anti-correlations, possibly by low-mass asymptotic giant branch stars. Lastly, we find that [Ce/Fe] ratios in M 54 are almost flat as a function of metrallicity. Unfortunately, Nd II is measured in only one star, which has been found to exhibit the modest enhancement, which is consistent with a moderate enrichment of s-process elements.

Furthermore, we report the serendipitous discovery of two N-enhanced stars identified within ∼7r_t from M 54, as shown in panel a of Fig. 1. Panel a of Fig. 2 shows the collection of [X/Fe] and [Fe/H] abundance ratios for the two newly identified N-rich stars beyond the tidal radius of M 54. Both stars exhibit very similar chemical-abundance patterns as those seen in the population of M 54. A plausible explanation is that both stars were previous members of M 54, from which they have been ejected. However, this possibility seems unlikely for one of these extra-tidal stars (2M18533777−3129187), which was ruled out as a possible member of M 54.

As can be appreciated from inspection of panels a–d of Fig. 1, the current position of 2M18533777−3129187 does not resemble the kinematic and astrometric properties (e.g., Antoja et al. 2020; Hayes et al. 2020) of Sgr+M 54 stars, nor the orbital path of Sgr[1]. It is also the most luminous star in our sample, making it a likely foreground star. The possibility that this star was disrupted from M 54 and deposited in the inner Galaxy seems unlikely, as the perigalacticon of M 54 is located

[1] The Sgr orbit was computed with the GravPot16 model, https://gravpot.utinam.cnrs.fr, by adopting the same model configurations as described in Fernández-Trincado et al. (2020b). For the Sgr center, we adopt the heliocentric distance $d_\odot$ = 26.5 kpc and heliocentric RV = 142 km s^{-1} from Vasiliev & Belokurov (2020), and proper motions from Gaia Collaboration (2018b): $\mu_\alpha \cos\delta$ = −2.692 mas yr^{-1} and μ_δ = −1.359 mas yr^{-1}, with uncertainties assumed on the order of 10% in $d_\odot$, RV, and proper motions.

well beyond the solar radius (see, e.g., Baumgardt et al. 2019). We conclude that 2M18533777−3129187 is a N-enhanced field star born in a different progenitor than M 54, but with a similar chemical-enrichment history to this cluster.

Aside from 2M18533777−3129187, there is another N-enhanced field star (2M18565969−3106454) located $\sim 5 \times r_t$ from the cluster center. This star exhibits a stellar atmosphere strongly enriched in nitrogen ([N/Fe] > +1.4) that is as extreme as M 54 stars and is accompanied by a very low carbon abundance ([C/Fe] < –0.7), and has discernible contributions from the *s*-process elements (Ce II). Since the [Al/Fe] ratio is > + 0.5, which is a typical value for stars in GCs and unlikely in dwarf galaxy populations, we conclude that 2M18565969−3106454 shares the same nucleosynthetic pathways of second-generation stars in M 54.

2M18565969−3106454 is a potential extra-tidal star with kinematics and astrometric properties similar to that of M 54 stars that exhibits unique chemical patterns comparable to that of genuine second-generation GC stars, which makes it very different from Sgr stars. On the other hand, N-rich stars are commonly observed to be more centrally concentrated in GCs (e.g. Dalessandro et al. 2019) and as a consequence they have a smaller probability of being tidally stripped. Thus, it is likely that the extra-tidal star could well be just a stripped M 54 star as many others in its surroundings. Our finding demonstrates that N-rich stars are a promising route for identifying the unambiguous chemical signatures of stars formed in GC-like environment that may lie immersed in the M 54+Sgr core and/or Sgr stream; our result also confirms or discards the possible association of GCs to the Sgr stream (Bellazzini et al. 2020).

Following the same methodology as described in Fernández-Trincado et al. (2021b), we compute the predicted number ($N_{\rm N-rich}$) of N-rich field stars observed in APOGEE-2 toward M 54/Sgr using the smooth halo density relations presented in Horta et al. (2021), and by adopting the same Monte Carlo implementation of the Von Neumann Rejection Technique (see, e.g., Press et al. 2002) as in Eq. (7) in Fernández-Trincado et al. (2015). We find the expected number of observed N-rich halo stars beyond $d_\odot \gtrsim 15$ kpc over the sky area of 1.5 degree radius centered in M 54, with both astrometric and kinematic properties as M 54 to be $N_{\rm N-rich} < 0.1$ (from 1000 Monte Carlo realizations). This yield a very low probability that the new identified extra-tidal N-rich star associated with M 54 is due to random fluctuations in the field. Furthermore, we also use the Besançon galactic model (Robin et al. 2003) and the `GravPot16` model (Fernández-Trincado et al. 2020e) to explore the expectations for a "default" MW along the RVs to the Sgr+M54 surrounding field beyond $d_\odot \gtrsim 15$ kpc. The "all" sample is dominated by halo kinematics with a negligible contribution from the thin and thick disk beyond RV $\gtrsim 120\,{\rm km\,s^{-1}}$. Thus, our MW simulated sample act to guide us in RV space, confirming that the kinematics of the newly identified extra-tidal N-rich star differs from the disk population, with low contribution from the expected halo.

5. Concluding remarks

We present a spectroscopic analysis for 20 out of 22 red giant stars that are members of M 54 from the internal APOGEE DR16 data set. This study doubles the sample of stars with spectroscopic measurements for this cluster, and the new post-APOGEE DR16 spectra achieve high $S/N > 70$, allowing the addition of new chemical species not examined in previous studies (e.g., Mészáros et al. 2020) in the *H*-band–APOGEE-2 footprint.

Overall, the chemical species re-examined in M 54 were found to be consistent with previous studies (Mészáros et al. 2020), although most of these species exhibit a large star-to-star scatter. We find that 15 out of the 20 stars investigated show a high [N/Fe] abundance ratio ([N/Fe] $\gtrsim +0.5$), confirming the prevalence of the MPs phenomenon in M 54. Both [Ni/Fe] and [Ti/Fe], not previously examined in Mészáros et al. (2020), were found to be in good agreement with measurements in the literature. In particular, we confirm the [Ti/Fe] ratio slightly increases as [Fe/H] increases, as was reported in Carretta et al. (2010). We also find a large spread in [Al/Fe], and the presence of a genuine second-generation star in M 54, which exhibits Mg deficiency ([Mg/Fe] < 0) accompanied by large enhancements in nitrogen and aluminum. In general, all chemical species examined in the M 54 members present distinguishable chemical behaviour compared with Sgr stars, suggesting a different chemical-evolution history that resembles other Galactic halo GCs at similar metallicity.

Furthermore, we report on the serendipitous discovery of a potential extra-tidal star toward the surrounding regions of the M 54+Sgr core, which exhibits a strong enrichment in nitrogen comparable to that seen in M 54 stars. As far as we know this is the first study reporting on the unambiguous chemical signatures of stars formed in GC-like environment into a nearby satellite dwarf galaxy around the MW. Finding out how many of such chemical unusual stars likely originated in GCs are present in dwarf galaxy systems helps us to understand the link between GCs and their stellar streams (see e.g., Bellazzini et al. 2020).

Acknowledgements. The author is grateful for the enlightening feedback from the anonymous referee. J.G.F-T is supported by FONDECYT No. 3180210. T.C.B. acknowledges partial support for this work from grant PHY 14-30152: Physics Frontier Center/JINA Center for the Evolution of the Elements (JINA-CEE), awarded by the US National Science Foundation. D.M. is supported by the BASAL Center for Astrophysics and Associated Technologies (CATA) through grant AFB 170002, and by project FONDECYT Regular No. 1170121. S.V. gratefully acknowledges the support provided by Fondecyt regular No. 1170518. D.G. gratefully acknowledges support from the Chilean Centro de Excelencia en Astrofísica y Tecnologías Afines (CATA) BASAL grant AFB-170002. D.G. also acknowledges financial support from the Dirección de Investigación y Desarrollo de la Universidad de La Serena through the Programa de Incentivo a la Investigación de Académicos (PIA-DIDULS). A.R.-L. acknowledges financial support provided in Chile by Agencia Nacional de Investigación y Desarrollo (ANID) through the FONDECYT project 1170476. B.B. acknowledges partial financial support from the Brazilian agencies CAPES-Financial code 001, CNPq, and FAPESP. This work has made use of data from the European Space Agency (ESA) mission *Gaia* (`http://www.cosmos.esa.int/gaia`), processed by the *Gaia* Data Processing and Analysis Consortium (DPAC, `http://www.cosmos.esa.int/web/gaia/dpac/consortium`). Funding for the DPAC has been provided by national institutions, in particular the institutions participating in the *Gaia* Multilateral Agreement. Funding for the Sloan Digital Sky Survey IV has been provided by the Alfred P. Sloan Foundation, the US Department of Energy Office of Science, and the Participating Institutions. SDSS- IV acknowledges support and resources from the Center for High-Performance Computing at the University of Utah. The SDSS web site is `www.sdss.org`. SDSS-IV is managed by the Astrophysical Research Consortium for the Participating Institutions of the SDSS Collaboration including the Brazilian Participation Group, the Carnegie Institution for Science, Carnegie Mellon University, the Chilean Participation Group, the French Participation Group, Harvard-Smithsonian Center for Astrophysics, Instituto de Astrofísica de Canarias, The Johns Hopkins University, Kavli Institute for the Physics and Mathematics of the Universe (IPMU)/University of Tokyo, Lawrence Berkeley National Laboratory, Leibniz Institut für Astrophysik Potsdam (AIP), Max-Planck-Institut für Astronomie (MPIA Heidelberg), Max-Planck-Institut für Astrophysik (MPA Garching), Max-Planck-Institut für Extraterrestrische Physik (MPE), National Astronomical Observatory of China, New Mexico State University, New York University, University of Notre Dame, Observatório Nacional/MCTI, The Ohio State University, Pennsylvania State University, Shanghai Astronomical Observatory, United Kingdom Participation Group, Universidad Nacional Autónoma de México, University of Arizona, University of Colorado Boulder, University of Oxford, University of Portsmouth, University of Utah, University of Virginia, University of Washington, University of Wisconsin, Vanderbilt University, and Yale University.

References

Abolfathi, B., Aguado, D. S., Aguilar, G., et al. 2018, ApJS, 235, 42
Ahumada, R., Allende Prieto, C., Almeida, A., et al. 2020, ApJS, 249, 3
Antoja, T., Ramos, P., Mateu, C., et al. 2020, A&A, 635, L3
Baumgardt, H., Hilker, M., Sollima, A., & Bellini, A. 2019, MNRAS, 482, 5138
Bekki, K. 2019, MNRAS, 490, 4007
Bellazzini, M., Ibata, R., Malhan, K., et al. 2020, A&A, 636, A107
Blanton, M. R., Bershady, M. A., Abolfathi, B., et al. 2017, AJ, 154, 28
Bowen, I. S., & Vaughan, A. H. J. 1973, Appl. Opt., 12, 1430
Carretta, E., Bragaglia, A., Gratton, R. G., et al. 2010, A&A, 520, A95
Correnti, M., Bellazzini, M., Ibata, R. A., Ferraro, F. R., & Varghese, A. 2010, ApJ, 721, 329
Cunha, K., Smith, V. V., Hasselquist, S., et al. 2017, ApJ, 844, 145
Dalessandro, E., Cadelano, M., Vesperini, E., et al. 2019, ApJ, 884, L24
de Boer, T. J. L., Belokurov, V., & Koposov, S. 2015, MNRAS, 451, 3489
Denissenkov, P. A., VandenBerg, D. A., Hartwick, F. D. A., et al. 2015, MNRAS, 448, 3314
Eisenstein, D. J., Weinberg, D. H., Agol, E., et al. 2011, AJ, 142, 72
Fernández-Trincado, J. G., Vivas, A. K., Mateu, C. E., et al. 2015, A&A, 574, A15
Fernández-Trincado, J. G., Robin, A. C., Moreno, E., et al. 2016, ApJ, 833, 132
Fernández-Trincado, J. G., Zamora, O., García-Hernández, D. A., et al. 2017, ApJ, 846, L2
Fernández-Trincado, J. G., Beers, T. C., Placco, V. M., et al. 2019a, ApJ, 886, L8
Fernández-Trincado, J. G., Beers, T. C., Tang, B., et al. 2019b, MNRAS, 488, 2864
Fernández-Trincado, J. G., Mennickent, R., Cabezas, M., et al. 2019c, A&A, 631, A97
Fernández-Trincado, J. G., Zamora, O., Souto, D., et al. 2019d, A&A, 627, A178
Fernández-Trincado, J. G., Beers, T. C., Minniti, D., et al. 2020a, ApJ, 903, L17
Fernández-Trincado, J. G., Beers, T. C., Minniti, D., et al. 2020b, A&A, 643, L4
Fernández-Trincado, J. G., Beers, T. C., & Minniti, D. 2020c, A&A, 644, A83
Fernández-Trincado, J. G., Minniti, D., Beers, T. C., et al. 2020d, A&A, 643, A145
Fernández-Trincado, J. G., Chaves-Velasquez, L., Pérez-Villegas, A., et al. 2020e, MNRAS, 495, 4113
Fernández-Trincado, J. G., Minniti, D., Souza, S. O., et al. 2021a, ApJ, 908, L42
Fernández-Trincado, J. G., Beers, T. C., Minniti, D., et al. 2021b, A&A, 647, A64
Freeman, K., & Bland-Hawthorn, J. 2002, ARA&A, 40, 487
Gaia Collaboration (Brown, A. G. A., et al.) 2018a, A&A, 616, A1
Gaia Collaboration (Helmi, A., et al.) 2018b, A&A, 616, A12
Gaia Collaboration (Brown, A. G. A., et al.) 2021, A&A, in press, https://doi.org/10.1051/0004-6361/202039657
García Pérez, A. E., Allende Prieto, C., Holtzman, J. A., et al. 2016, AJ, 151, 144
Gunn, J. E., Siegmund, W. A., Mannery, E. J., et al. 2006, AJ, 131, 2332
Gustafsson, B., Edvardsson, B., Eriksson, K., et al. 2008, A&A, 486, 951
Hanke, M., Koch, A., Prudil, Z., Grebel, E. K., & Bastian, U. 2020, A&A, 637, A98
Harris, W. E. 1996, AJ, 112, 1487
Hasselquist, S., Shetrone, M., Cunha, K., et al. 2016, ApJ, 833, 81
Hasselquist, S., Shetrone, M., Smith, V., et al. 2017, ApJ, 845, 162
Hasselquist, S., Carlin, J. L., Holtzman, J. A., et al. 2019, ApJ, 872, 58
Hayes, C. R., Majewski, S. R., Hasselquist, S., et al. 2020, ApJ, 889, 63
Holtzman, J. A., Shetrone, M., Johnson, J. A., et al. 2015, AJ, 150, 148
Holtzman, J. A., Hasselquist, S., Shetrone, M., et al. 2018, AJ, 156, 125
Horta, D., Mackereth, J. T., Schiavon, R. P., et al. 2021, MNRAS, 500, 5462
Huang, K.-W., & Koposov, S. E. 2021, MNRAS, 500, 986
Ibata, R. A., Gilmore, G., & Irwin, M. J. 1994, Nature, 370, 194
Ibata, R., Irwin, M., Lewis, G. F., & Stolte, A. 2001, ApJ, 547, L133
Jönsson, H., Allende Prieto, C., Holtzman, J. A., et al. 2018, AJ, 156, 126
Jönsson, H., Holtzman, J. A., Allende Prieto, C., et al. 2020, AJ, 160, 120
Karlsson, T., Bland-Hawthorn, J., Freeman, K. C., & Silk, J. 2012, ApJ, 759, 111
Law, D. R., & Majewski, S. R. 2010, ApJ, 718, 1128
Law, D. R., Johnston, K. V., & Majewski, S. R. 2005, ApJ, 619, 807
Li, J., Fellow, L., Liu, C., et al. 2019, ApJ, 874, 138
Majewski, S. R., Skrutskie, M. F., Weinberg, M. D., & Ostheimer, J. C. 2003, ApJ, 599, 1082
Majewski, S. R., Schiavon, R. P., Frinchaboy, P. M., et al. 2017, AJ, 154, 94
Massari, D., Koppelman, H. H., & Helmi, A. 2019, A&A, 630, L4
Masseron, T., Merle, T., & Hawkins, K. 2016, BACCHUS: Brussels Automatic Code for Characterizing High accUracy Spectra
Mateo, M., Mirabal, N., Udalski, A., et al. 1996, ApJ, 458, L13
McWilliam, A., Wallerstein, G., & Mottini, M. 2013, ApJ, 778, 149
Mészáros, S., Masseron, T., García-Hernández, D. A., et al. 2020, MNRAS, 492, 1641
Milone, A. P., Piotto, G., Renzini, A., et al. 2017, MNRAS, 464, 3636
Nataf, D. M., Wyse, R. F. G., Schiavon, R. P., et al. 2019, AJ, 158, 14
Newberg, H. J., Yanny, B., Grebel, E. K., et al. 2003, ApJ, 596, L191
Nidever, D. L., Holtzman, J. A., Allende Prieto, C., et al. 2015, AJ, 150, 173
Pancino, E., Romano, D., Tang, B., et al. 2017, A&A, 601, A112
Plez, B. 2012, Turbospectrum: Code for spectral synthesis
Press, W. H., Teukolsky, S. A., Vetterling, W. T., & Flannery, B. P. 2002, Numerical Recipes in C++ : the Art of Scientific Computing
Ramos, P., Mateu, C., Antoja, T., et al. 2020, A&A, 638, A104
Recio-Blanco, A., Rojas-Arriagada, A., de Laverny, P., et al. 2017, A&A, 602, L14
Renzini, A., D'Antona, F., Cassisi, S., et al. 2015, MNRAS, 454, 4197
Robin, A. C., Reylé, C., Derrière, S., & Picaud, S. 2003, A&A, 409, 523
Schiavon, R. P., Zamora, O., Carrera, R., et al. 2017, MNRAS, 465, 501
Shetrone, M., Bizyaev, D., Lawler, J. E., et al. 2015, ApJS, 221, 24
Sills, A., Dalessandro, E., Cadelano, M., Alfaro-Cuello, M., & Kruijssen, J. M. D. 2019, MNRAS, 490, L67
Smith, V. V., Cunha, K., Shetrone, M. D., et al. 2013, ApJ, 765, 16
Tang, B., Fernández-Trincado, J. G., Geisler, D., et al. 2018, ApJ, 855, 38
Ting, Y.-S., Conroy, C., Rix, H.-W., & Cargile, P. 2019, ApJ, 879, 69
Totten, E. J., & Irwin, M. J. 1998, MNRAS, 294, 1
Vasiliev, E., & Belokurov, V. 2020, MNRAS, 497, 4162
Vasiliev, E., Belokurov, V., & Erkal, D. 2021, MNRAS, 501, 2279
Villanova, S., Monaco, L., Moni Bidin, C., & Assmann, P. 2016, MNRAS, 460, 2351
Wilson, J. C., Hearty, F., Skrutskie, M. F., et al. 2012, in Ground-based and Airborne Instrumentation for Astronomy IV, eds. I. S. McLean, S. K. Ramsay, & H. Takami, SPIE Conf. Ser., 8446, 84460
Wilson, J. C., Hearty, F. R., Skrutskie, M. F., et al. 2019, PASP, 131, 055001
Yuan, Z., Chang, J., Beers, T. C., & Huang, Y. 2020, ApJ, 898, L37
Zasowski, G., Cohen, R. E., Chojnowski, S. D., et al. 2017, AJ, 154, 198

Appendix A: Spectrum of N-rich stars

Figure A.1 shows an example of the local thermodynamic equilibrium (LTE) –BACCHUS spectral synthesis of selected $^{12}C^{14}N$ lines for the two newly identified N-rich stars beyond the tidal radius of M 54. The black squares represent the observed spectrum and the solid red line is the best abundance fit.

We also provide our results in three tables. The first table, which can be found in Table A.1 contains the atmospheric parameters and abundance ratios, while Table A.2 list the final errors in [Fe/H] and [X/Fe]. Table A.3 contains the main physical properties of our sample.

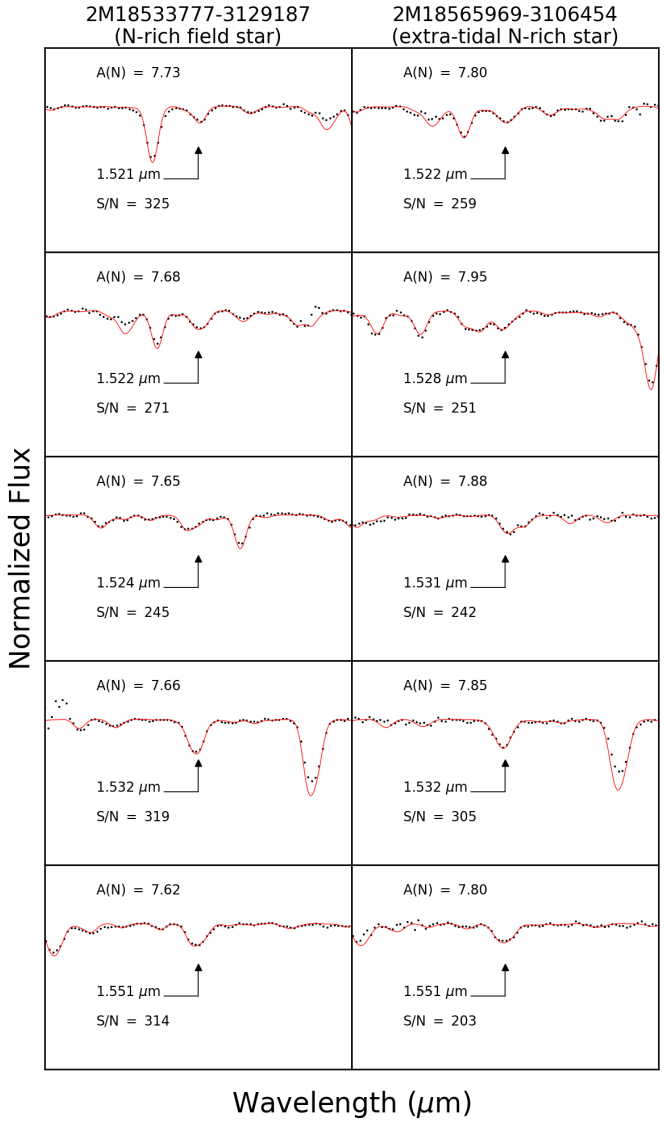

Fig. A.1. Detection of $^{12}C^{14}N$ lines. Spectral synthesis for the determination of nitrogen abundances for two N-rich stars beyond the tidal radius of M 54. Each panel shows the best-fit syntheses (red lines) from BACCHUS compared to the observed spectra (black squares) of selected $^{12}C^{14}N$ lines (grey arrows).

Table A.1. Elemental abundances of our sample.

APOGEE ID	$T_{\rm eff}$ [K]	log g [cgs]	[M/H]	ξ_t km s^{-1}	[C/Fe]	[N/Fe]	[O/Fe]	[Mg/Fe]	[Al/Fe]	[Si/Fe]	[K/Fe]	[Ca/Fe]	[Ti/Fe]	[Fe/H]	[Ni/Fe]	[Ce/Fe]	[Nd/Fe]
N-rich field star																	
2M18533777−3129187	4158	1.23	−1.35	1.8	−0.60	+1.21	+0.22	+0.21	+0.58	+0.39	+0.07	+0.14	+0.31	−1.33	−0.01	+0.22	+0.30
Extra-tidal N-rich star																	
2M18565969−3106454	4211	1.33	−1.37	2.2	−0.72	+1.44	+0.19	+0.03	+0.51	+0.26	+0.13	+0.11	+0.28	−1.39	−0.06	+0.24	…
M 54 stars																	
2M18544275−3029012	4480	1.08	−1.40	1.8	…	…	…	+0.38	+0.22	+0.23	…	+0.32	+0.17	−1.37	−0.05	…	…
2M18544848−3031588	4625	1.35	−1.39	1.9	−0.38	+1.06	+0.96	+0.24	−0.24	+0.26	+0.10	+0.23	+0.48	−1.42	+0.20	+0.21	…
2M18545303−3024220	4999	2.13	−0.69	1.6	…	…	…	+0.29	−0.08	+0.26	+0.16	…	…	−1.32	+0.27	…	…
2M18545434−3028458	5013	2.16	−0.79	2.5	+0.29	+1.33	+1.30	+0.09	+0.16	+0.26	+0.16	…	+0.62	−1.05	−0.01	…	…
2M18545470−3027044	4271	0.69	−1.31	2.6	…	+0.59	+0.77	+0.17	+0.13	+0.21	−0.09	+0.23	+0.46	−1.41	−0.02	+0.28	…
2M18545774−3025574	4110	0.37	−1.37	2.9	…	+0.35	+0.48	+0.03	+0.02	+0.14	+0.15	+0.23	+0.17	−1.39	+0.05	+0.03	…
2M18545920−3028403	4360	0.85	−1.42	2.0	−0.43	+1.00	+0.68	+0.16	+0.24	+0.20	+0.11	+0.13	+0.15	−1.43	+0.04	+0.17	+0.44
2M18550076−3034068	4560	1.23	−1.48	1.5	−0.24	…	+0.76	+0.26	−0.37	+0.24	…	+0.23	+0.10	−1.39	−0.01	+0.41	…
2M18550247−3031314	4831	1.76	−1.11	2.5	…	…	…	+0.13	−0.17	+0.31	+0.33	…	…	−1.32	+0.51	…	…
2M18550293−3029523	4851	1.8	−1.09	1.7	…	…	…	+0.22	…	+0.39	…	+0.29	…	−1.39	+0.28	…	…
2M18550560−3026332	4477	1.07	−0.54	2.5	−0.14	+2.20	…	…	+0.86	+0.43	+0.44	…	+0.77	−1.09	−0.04	…	…
2M18550623−3030561	4584	1.28	−1.11	2.3	−0.24	+1.48	+0.82	+0.22	+0.54	+0.27	−0.00	+0.32	+0.27	−1.31	+0.00	+0.38	…
2M18550740−3026052	4233	0.62	−1.32	2.0	−0.51	+1.00	+0.64	+0.24	−0.21	+0.27	+0.06	+0.22	+0.18	−1.42	+0.09	…	…
2M18550843−3029045	4238	0.63	−0.88	2.7	−0.27	+1.89	+0.82	+0.29	+0.41	+0.29	+0.28	+0.39	+0.52	−1.12	+0.02	…	…
2M18551026−3033406	4110	0.37	−1.36	2.9	−0.72	+1.35	+0.45	+0.04	+0.36	+0.16	−0.01	+0.14	+0.13	−1.46	+0.01	+0.12	…
2M18551034−3027105	4463	1.05	−1.14	1.7	−0.48	+0.99	+0.77	+0.20	−0.12	+0.20	−0.12	+0.14	…	−1.21	−0.01	…	…
2M18551061−3029597	4837	1.77	−1.17	1.5	…	…	…	+0.11	+0.63	+0.23	+0.30	+0.35	+0.30	−1.28	+0.19	…	…
2M18551152−3025352	4961	2.05	−1.38	1.7	…	…	…	+0.32	−0.19	+0.25	…	+0.33	+0.50	−1.22	+0.00	…	…
2M18551416−3028548	4161	0.48	−1.32	2.7	−0.31	+0.90	−0.40	−0.02	+0.90	+0.24	+0.21	+0.26	+0.26	−1.27	−0.02	+0.15	…
2M18551535−3024142	4084	0.32	−1.31	2.7	−0.57	+0.67	+0.53	+0.03	−0.31	+0.15	+0.11	+0.20	+0.08	−1.29	−0.04	+0.07	…
2M18551672−3027508	4695	1.49	−0.74	2.2	…	+1.28	…	…	+0.24	+0.55	+0.54	…	…	−1.28	+0.17	…	…
2M18552982−3028545	4228	0.61	−1.43	2.0	−0.64	+0.58	+0.41	+0.19	−0.20	+0.12	−0.01	+0.22	+0.13	−1.18	−0.08	+0.02	…

Table A.2. Final errors in [Fe/H] and [X/Fe].

APOGEE ID	$\sigma_{\rm [C/Fe]}$	$\sigma_{\rm [N/Fe]}$	$\sigma_{\rm [O/Fe]}$	$\sigma_{\rm [Mg/Fe]}$	$\sigma_{\rm [Al/Fe]}$	$\sigma_{\rm [Si/Fe]}$	$\sigma_{\rm [K/Fe]}$	$\sigma_{\rm [Ca/Fe]}$	$\sigma_{\rm [Ti/Fe]}$	$\sigma_{\rm [Fe/H]}$	$\sigma_{\rm [Ni/Fe]}$	$\sigma_{\rm [Ce/Fe]}$	$\sigma_{\rm [Nd/Fe]}$
N-rich field star													
2M18533777−3129187	0.03	0.06	0.17	0.07	0.04	0.06	0.04	0.11	0.12	0.05	0.11	0.08	0.04
Extra-tidal N-rich star													
2M18565969−3106454	0.03	0.08	0.20	0.07	0.06	0.06	0.04	0.15	0.11	0.05	0.11	0.09	…
M 54 stars													
2M18544275−3029012	…	…	…	0.09	0.07	0.09	…	0.16	0.12	0.07	0.12	…	…
2M18544848−3031588	0.05	0.14	0.16	0.08	0.06	0.08	0.05	0.13	0.09	0.06	0.15	0.10	…
2M18545303−3024220	…	…	…	0.10	0.08	0.21	0.08	…	…	0.09	0.11	…	…
2M18545434−3028458	0.04	0.09	0.09	0.06	0.09	0.06	0.06	…	0.12	0.04	0.11	…	…
2M18545470−3027044	…	0.10	0.17	0.08	0.08	0.07	0.08	0.07	0.07	0.05	0.07	0.11	…
2M18545774−3025574	…	0.08	0.13	0.08	0.13	0.07	0.06	0.06	0.11	0.06	0.12	0.12	…
2M18545920−3028403	0.06	0.07	0.04	0.08	0.07	0.06	0.06	0.12	0.08	0.04	0.11	0.07	0.04
2M18550076−3034068	0.06	…	0.13	0.08	0.05	0.08	…	0.12	0.09	0.06	0.12	0.06	…
2M18550247−3031314	…	…	…	0.09	0.07	0.13	0.07	…	…	0.08	0.11	…	…
2M18550293−3029523	…	…	…	0.14	…	0.22	…	0.15	…	0.09	0.08	…	…
2M18550560−3026332	0.06	0.17	…	…	0.07	0.07	0.07	…	0.08	0.07	0.12	…	…
2M18550623−3030561	0.06	0.08	0.06	0.08	0.07	0.05	0.06	0.21	0.09	0.07	0.08	0.07	…
2M18550740−3026052	0.10	0.08	0.15	0.09	0.10	0.12	0.05	0.13	0.13	0.06	0.12	…	…
2M18550843−3029045	0.04	0.10	0.20	0.11	0.08	0.06	0.05	0.15	0.10	0.11	0.05	…	…
2M18551026−3033406	0.07	0.07	0.07	0.07	0.14	0.05	0.07	0.11	0.07	0.12	0.12	0.08	…
2M18551034−3027105	0.07	0.08	0.05	0.07	0.09	0.06	0.05	0.09	…	0.05	0.13	…	…
2M18551061−3029597	…	…	…	0.08	0.11	0.08	0.07	0.07	0.13	0.06	0.13	…	…
2M18551152−3025352	…	…	…	0.08	0.06	0.08	…	0.12	0.10	0.07	0.12	…	…
2M18551416−3028548	0.04	0.07	0.18	0.07	0.07	0.08	0.05	0.15	0.15	0.08	0.14	0.09	…
2M18551535−3024142	0.05	0.08	0.08	0.05	0.09	0.08	0.05	0.05	0.11	0.07	0.09	0.09	…
2M18551672−3027508	…	0.11	…	…	0.08	0.16	0.09	…	…	0.08	0.12	…	…
2M18552982−3028545	0.06	0.05	0.09	0.15	0.07	0.08	0.06	0.08	0.07	0.05	0.09	0.08	…

Table A.3. Astrometric and kinematic properties of our sample.

APOGEE ID	RUWE	$\mu_\alpha \cos(\delta) \pm \Delta$ mas yr^{-1}	$\mu_\delta \pm \Delta$ mas yr^{-1}	G [mag]	$G_{\rm BP}$ [mag]	$G_{\rm RP}$ [mag]	RV km s^{-1}	RV-scatter km s^{-1}	S/N pixel^{-1}	# Visits
N-rich field star									pixel^{-1}	
2M18533777−3129187	0.9	0.001 ± 0.016	-4.150 ± 0.013	12.79	13.62	11.91	181.02	0.26	402	6
Extra-tidal N-rich star										
2M18565969−3106454	0.9	-2.701 ± 0.027	-1.336 ± 0.023	14.75	15.59	13.86	134.75	0.55	225	12
M 54 stars										
2M18544275−3029012	1.0	-2.667 ± 0.040	-1.357 ± 0.033	15.55	16.27	14.71	137.07	0.33	51	4
2M18544848−3031588	1.1	-2.686 ± 0.037	-1.356 ± 0.030	15.17	15.91	14.32	141.74	0.34	172	12
2M18545303−3024220	0.8	-2.584 ± 0.052	-1.430 ± 0.045	16.27	16.91	15.49	147.14	0.91	53	10
2M18545434−3028458	1.1	-2.694 ± 0.052	-1.440 ± 0.045	15.72	16.33	14.85	142.11	0.42	109	12
2M18545470−3027044	1.4	-2.412 ± 0.035	-1.345 ± 0.030	14.60	15.44	13.68	131.88	1.16	266	12
2M18545774−3025574	1.1	-2.717 ± 0.029	-1.321 ± 0.025	14.68	15.54	13.75	148.86	1.76	262	12
2M18545920−3028403	1.1	-2.800 ± 0.040	-1.374 ± 0.035	14.88	15.54	13.92	145.79	0.71	217	12
2M18550076−3034068	0.9	-2.685 ± 0.036	-1.494 ± 0.030	15.35	16.07	14.52	149.07	0.38	118	6
2M18550247−3031314	1.0	-2.625 ± 0.049	-1.310 ± 0.040	16.10	16.76	15.33	138.48	0.77	82	12
2M18550293−3029523	1.0	-2.526 ± 0.045	-1.230 ± 0.037	15.82	16.30	14.89	141.96	0.49	115	12
2M18550560−3026332	0.9	-2.617 ± 0.045	-1.345 ± 0.038	15.93	16.60	15.12	143.86	0.29	93	10
2M18550623−3030561	1.0	-2.832 ± 0.038	-1.366 ± 0.032	15.57	16.29	14.74	135.17	0.31	136	12
2M18550740−3026052	1.0	-2.658 ± 0.028	-1.243 ± 0.023	14.82	15.65	13.94	132.96	0.95	93	4
2M18550843−3029045	1.0	-2.557 ± 0.038	-1.340 ± 0.031	15.46	16.16	14.54	135.85	0.35	158	12
2M18551026−3033406	1.1	-2.644 ± 0.027	-1.407 ± 0.021	14.49	15.41	13.54	142.01	0.74	309	12
2M18551034−3027105	1.0	-2.682 ± 0.037	-1.379 ± 0.030	15.44	16.19	14.60	154.11	0.31	106	6
2M18551061−3029597	1.1	-2.888 ± 0.054	-1.325 ± 0.044	16.07	16.65	15.24	147.11	0.94	78	11
2M18551152−3025352	1.0	-2.665 ± 0.053	-1.407 ± 0.044	16.22	16.74	15.35	146.85	0.62	73	10
2M18551416−3028548	1.1	-2.675 ± 0.031	-1.342 ± 0.026	14.98	15.80	14.10	139.67	0.38	208	12
2M18551535−3024142	1.0	-2.683 ± 0.029	-1.403 ± 0.023	14.74	15.62	13.82	151.11	1.01	230	12
2M18551672−3027508	0.9	-2.692 ± 0.043	-1.407 ± 0.035	15.80	16.44	15.00	140.11	0.94	76	11
2M18552982−3028545	0.9	-2.689 ± 0.033	-1.292 ± 0.028	15.15	15.96	14.27	135.09	0.38	192	12

Notes. The last two columns indicate the typical S/N of the spectra and number of APOGEE visits.